Radiation Induced Attenuation and Luminescence Study in Radioluminescent Optical Fibers

Nourdine Kerboub, *Member, IEEE*, Diego Di Francesca, Adriana Morana, *Member, IEEE*, Hicham El Hamzaoui, Youcef Ouerdane, Géraud Bouwmans, Andy Cassez, Aziz Boukenter, Bruno Capoen, Emmanuel Marin, Mohamed Bouazaoui, Daniel Ricci, Ruben Garcia Alia, *Member, IEEE*, Julien Mekki, Olivier Gilard, Nicolas Balcon, and Sylvain Girard, *Senior Member, IEEE*

***Abstract*— We present the experimental characterization of both radiation induced attenuation (RIA) and radioluminescence (RL) of differently doped optical fiber (OF) radiation sensors. We present data for different sample lengths and total ionizing dose (TID) up to 600 kGy (SiO_2) under X-rays. Combined RIA and RL responses are used to attempt explaining the variation of the RL signal with TID on those fibers.**

***Index Terms*— Cerium, dosimetry, OF sensors, optical fibers (OFs), radiation detection, radiations, radioluminescence (RL), silica glass, space applications, space radiation, X-rays.**

I. Introduction

RADIATION is a major concern in many specific environments, such as high energy physics facilities, spacecrafts, nuclear power plants, and the medical sector. Not only does it affect humans but it also impacts electronic systems, threatening the normal functioning of devices. Silica-based optical fibers (OFs) can also be subjected to different effects influencing their optical performances. The major observable effect is the radiation induced attenuation (RIA) [1]. RIA evolution depends mainly on the environmental conditions, the chemical composition of the fiber itself, and wavelength domain [1]. In some harsh environments, mostly where displacement damages in the silica matrix add up to ionization ones (high neutron fluence for instance), radiation induced refractive index change (RIRIC) [2], [3] is also possible. In addition, radiation can induce the emission of light from the OF material. This effect is known as radiation induced emission (RIE), which occurs when a particle, traveling through the material, generates the emission of photons through Cerenkov or via the excitation/photoemission of point defects and/or active doping centers [radioluminescence (RL)] [4].

On the one hand, these phenomena can be detrimental to the performance of OF-based systems in harsh environments [5] and many studies exist on the hardening techniques of OFs for data links or sensing applications [1], [6], [7]. On the other hand, the same effects are an asset for the monitoring of radiation levels and dosimetry applications. In particular, OFs can be characterized and used as radiation monitor/dosimeter if their behavior fulfills some specific requirements [8].

In this study, some specialty OFs are investigated to target dosimetry applications, in accelerators and space. These sol–gel silica-based OFs material were previously studied and proved having interesting detection efficiency under irradiation at room temperature (RT) [9], [10], [11], [12], [13]. For instance, a Ce-doped glassy rod showed a linear response versus dose rate up to 30 Gy(SiO_2)/s [14]. In addition, Cu- [12] and Gd-doped [15] as well as CuCe-codoped fiber materials [16] were developed and showed interesting features, such as high detection efficiency and linearity of the RL signal with the dose rate. It is important to mention that those fiber material are radioluminescent under any kind of ionizing particles and were tested under X-rays, gamma-rays, and proton beam [12]. The PhLAM Laboratory (Lille, France) developed silica-doped OFs based on those materials. These fibers are composed of a central doped core surrounded by a pure silica cladding. They have an outer diameter of about 125 μm, while the doped core section has a diameter of about 50 μm.

The tested fibers trigger interest in the accelerator sector because they potentially allow for the monitoring of time-dependent radiation environments within the accelerator complex of CERN, as well as level of radiation in shielded areas and experiments [17]. At CERN, we can expect radiation levels in the range up to the MGy level over several years, depending on the location, as well as dose rate up to 10^{-1} Gy/s.

Manuscript received 4 January 2023; revised 23 January 2023; accepted 7 February 2023. Date of publication 16 February 2023; date of current version 16 August 2023. This work was supported in part by the Laboratoire d'Excellence Centre Européen pour les Mathématiques, la Physique et leurs interactions (CEMPI) under Grant ANR-11-LABX-0007, in part by the Equipex Flux under Grant ANR-11-EQPX-0017, and in part by the Ministry of Higher Education and Research, Hauts de France Council and European Regional Development Fund (ERDF) through the Contrat de Projets Etat-Region (CPER Photonics for Society P4S).

Nourdine Kerboub is with CERN, 1211 Geneva, Switzerland, also with the Laboratoire Hubert Curien, University of Lyon, 42000 Saint-Étienne, France, and also with CNES, 31400 Toulouse, France (e-mail: nourdine.kerboub@cern.ch).

Diego Di Francesca, Daniel Ricci, and Ruben Garcia Alia are with CERN, 1211 Geneva, Switzerland.

Adriana Morana, Youcef Ouerdane, Aziz Boukenter, Emmanuel Marin, and Sylvain Girard are with the Laboratoire Hubert Curien, University of Lyon, 42000 Saint-Étienne, France.

Hicham El Hamzaoui, Géraud Bouwmans, Andy Cassez, Bruno Capoen, and Mohamed Bouazaoui are with CNRS, UMR8523-Physique des Lasers, Atomes et Molécules (PhLAM), CERLA/IRCICA, University of Lille, 59000 Lille, France.

Julien Mekki, Olivier Gilard, and Nicolas Balcon are with CNES, 31400 Toulouse, France.

Color versions of one or more figures in this article are available at https://doi.org/10.1109/TNS.2023.3246239.

Digital Object Identifier 10.1109/TNS.2023.3246239

Furthermore, the investigated sensors are also good candidates for space applications because of their high sensitivity enabling low dose rate levels monitoring in manned and unmanned missions. To provide such detection capabilities, these sensors must be able to withstand the harsh space environment characterized by total ionizing dose (TID) reaching up to 5 kGy (most of the time in between 100 and 500 Gy), dose rate within 10^{-9}–10^{-7} Gy/s, and temperature in the range -200 °C to $+300$ °C (outside of the satellite with no thermal control). For instance, such sensors could be used to provide an early detection of radiation level increase due to solar eruptions [18], allowing mitigating measures for sensitive equipment [19], [20] (temporary shutdown for instance) or humans (access to better-shielded areas of the spacecraft).

The real-time monitoring of the dose rate through the RL is directly related to the linearity of the RL level with respect to the dose rate. Consequently, it should be verified that this dependence is strictly linear and not affected by spurious mechanisms. For example, it is known that the RL level can increase during irradiation at a constant dose rate. This effect is called bright burn effect (BBE) [21]. This mechanism is described by the detrapping of electrons staying at energy levels with higher activation energy than the radioluminescent trap levels [22]. A significant temperature dependence of the RL was discovered and documented in [23], which defines the need of temperature calibration in certain environments. Such a temperature dependence was measured in glassy rods. All the tests included in this study are performed at RT (approximatively 22 °C), with a temperature variation small enough to have a negligible impact on the RL with regard to the temperature effects measured in [23].

To summarize, from the CERN application point of view, the main point of concern is the BBE, while the temperature dependence impact remains limited in most intended applications. From the space application standpoint, temperature effects are a major concern even though the BBE is still a major effect. Indeed, we have observed in a dataset not included in this study that 50 Gy on a pristine sample is enough to induce 5% BBE effect on the RL signal.

II. Sensors and Method

A. Silica Glass Sensors

The OF samples were prepared at the PhLAM Laboratory, within the FiberTech Lille platform, via the sol–gel technique. This latter allows to conceive waveguides with exotic composition not always accessible through chemical vapor deposition processes. Some cylindrical porous silica monoliths were synthetized, then soaked in cerium salts based solution [14], dried before densification at 1200 °C under helium atmosphere to increase the Ce^{3+} concentration [24], and thus the RL efficiency. This sol–gel process is used to produce Ce-doped fiber and repeated using other dopants than cerium (Cu and Gd) to produce the other fibers included in this study. The concentration of cerium ions in the Ce-doped and CuCe-doped fiber was estimated around 300 ppm, while copper ions in Cu-doped and CuCe-codoped was estimated to be around 250 ppm via electron microprobe analysis [16].

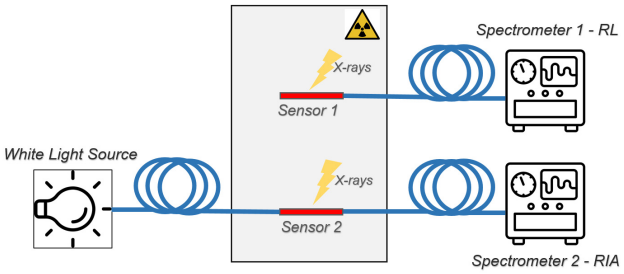

Fig. 1. Experimental setup implemented, for RL and RIA measurements. Optical fibers under test (FUT) are 1 or 5 cm long, and fusion-spliced to a 2–3-m RH-MM transport fiber toward spectrometers to measure either RIA or RL response of the FUT.

The obtained cylinder was then drawn into a thin rod and sleeved with a pure silica clad before being drawn a second time to a cane. Finally, this silica preform was drawn at 2000 °C to obtain a 125-μm-diameter fiber, with a 50-μm core diameter which is the sensitive area. The final steps of the manufacturing included a coating with a low refractive index polymer (DeSolite[1] DF-0016) to ensure the guiding properties of the fiber as well as protective polymer for mechanical strengthening.

B. Experimental Setup

For the experimental part of the study, we use two spectrometers: a QE65000 and a Jaz both from ocean optics. These are both UV–Vis–NIR spectrometers. We also make use of a DH-2000-BAL from ocean optics as a white light source (WLS). A variable multimode optical attenuator (not reported in Fig. 1) is used to reduce the light power injected in the sensor 2 fiber, to limit the photobleaching effect. The light power used in the RIA test is lower than 10 μW.

As described in Fig. 1, we run simultaneously the two spectrometers, and each of them connected to an uncoated pristine sample of FUT via a radiation hardened multimode (RH-MM) transport fiber. This fiber is fusion-spliced to the sample and the length of the sample adjusted for each experiment. The Jaz spectrometer is dedicated to the RL study. The ocean optics QE65000 spectrometer is used to measure the RIA in the second sample. For each experiment, sample one and sample two have the same length, within 1-mm error.

For all experiments, we apply the same irradiation time sequence: 8 h 20 min of irradiation, followed by a 5-h long recovery (no radiation) and finally a last 1-h long irradiation. The reason to perform a second short irradiation is to observe the evolution of the RL and RIA when the fiber has already been irradiated to be compared with the pristine fiber.

The samples are placed in the LABHX machine (at Hubert Curien Laboratory), which provides an irradiation area of 10 × 10 cm^2 under 40-keV average energy X-rays, emitted via a tube operated at 100 kV. In the rest of this work, all reported dose rates are in SiO_2. We expect a 10% accuracy on the dose rate. To investigate the RL and RIA responses for different fiber lengths and dose rates on the Ce-, Cu-, and Gd-doped

[1]Registered trademark.

TABLE I

EXPERIMENTAL CONDITIONS OF THE RL AND RIA MEASUREMENTS USED FOR Ce-, Cu-, AND Gd-DOPED AND CuCe-CODOPED FIBERS

Sample Length (cm)	Dose rate (Gy/s)	Minimal TID (kGy)
1	20	600
1	5	150
5	5	150
5	0.5	15

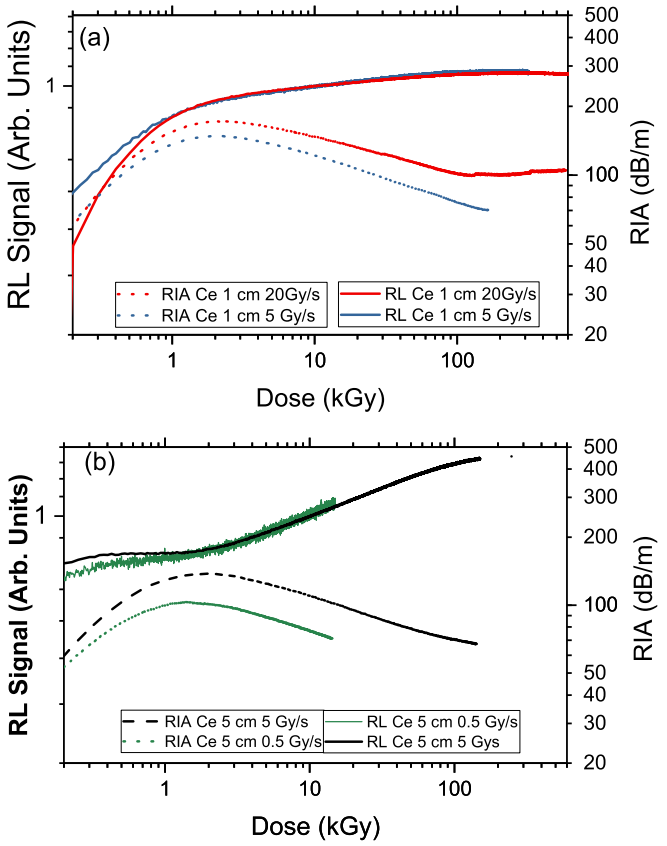

Fig. 2. RL and RIA measurements at 500 nm versus dose (at two different dose rates) on Ce-doped OF for (a) 1-cm-long and (b) 5-cm-long samples. RL data are normalized to the response at 10 kGy. Both RIA and RL are plotted in logarithmic scales.

and CuCe-codoped fibers, we carry out the tests according to the set of conditions presented in Table I.

III. EXPERIMENTAL RESULTS

In the rest of this work, we present the results of the RL and RIA measurements performed on the Ce-, Cu-, and Gd-doped and CuCe-codoped fibers. We report them in the following way: panel (a) in top part of the figure—we directly compare the measurements of RL and RIA performed on 1-cm-long samples, at 5 and 20 Gy/s. In panel (b) in the bottom part of the figure, we show the measurements performed on 5-cm-long samples at 5 and 0.5 Gy/s.

We normalize the RL signal to its amplitude at 10 kGy (arbitrary choice), to be able to compare the dynamics across different experiments. In the same figure, we plot on a second y-axis, the RIA measurement (same sample length), under the same irradiation condition. Both the RL and RIA are spectral measurements thus, to plot the evolution of the RL and RIA, we choose to plot the signal averaged around the wavelength of the maximum amplitude of the RL emission band of each fiber.

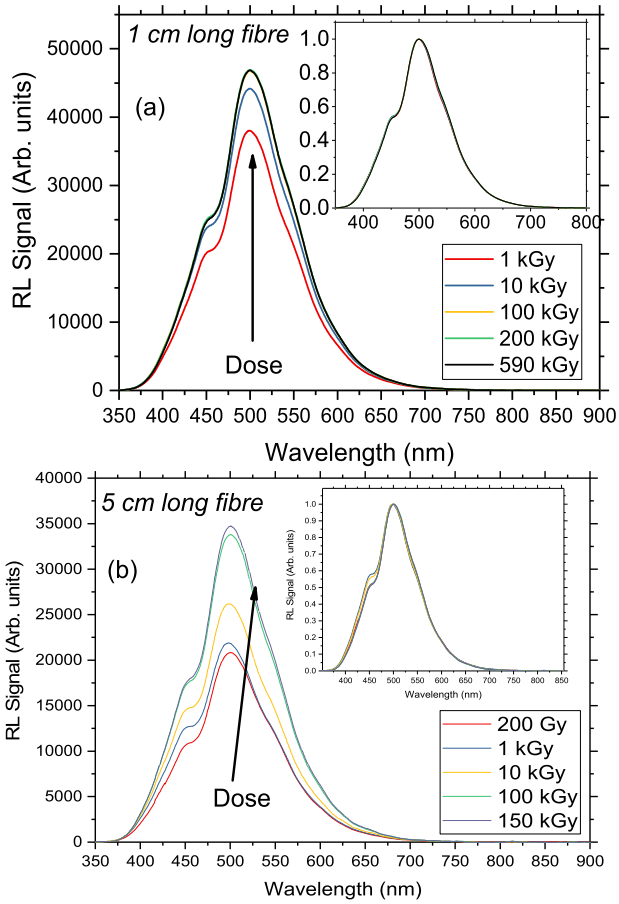

Fig. 3. RL spectrum measured on Ce-doped fiber for different TID levels shown as (a) 1-cm-long sample at 20 Gy/s and (b) 5-cm-long Ce-doped fiber at 5 Gy/s. Data are normalized to their own maximum amplitude in the insets.

A. Ce-Doped Fiber RL and RIA Measurements

First, we performed the investigations on the Ce-doped fiber, for which we plot the results in Fig. 2. All the data are measured by averaging the signal over 5 nm around 500 nm, which is close to the maximum of the RL emission band of this fiber. In the case of 1-cm-long measurements, we can observe that the RL signal increases significantly until a TID of a few kGy and then reaches a saturation value above 100 kGy.

The saturation/stabilization of the RL signal maintains itself within 0.2% from 100 kGy until at least 600 kGy. In parallel to the RL, we observe an increase of the RIA, until a maximum value located around a TID of 2 kGy. After that, the RIA (in dB/m) decreases slowly and stabilizes after 100 kGy within 1.5%. For 5-cm-long samples reported in Fig. 2(b), the RL signal increases at the beginning of the irradiation and then decreases to a flex point at 2 kGy, before increasing again until the end of the irradiation. We also noted that the maximum amplitude measured for the 1-cm experiment under 20 Gy/s is 5×10^4 counts (arbitrary units), whereas we reach 3.5×10^4

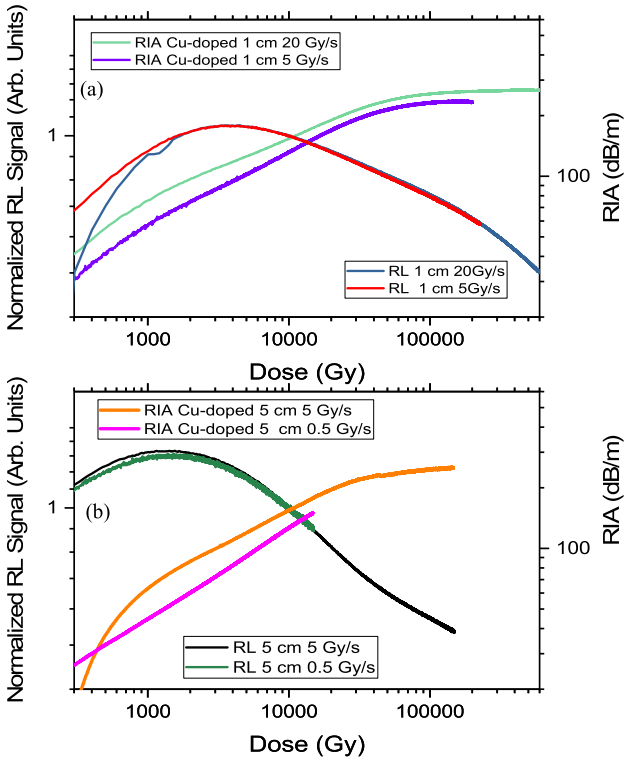

Fig. 4. RL and RIA measurements at 550 nm versus dose on Cu-doped OF for (a) 1-cm-long and (b) 5-cm-long sample. RL data are normalized to the response at 10 kGy. Both RIA and RL presented in logarithmic scales.

counts (arbitrary units) for the 5 cm with 5 Gy/s. We would expect in the second case 6.2×10^4 counts, but we can explain the mismatch by self-absorption of the emitted light in the 5-cm-long sample.

A conclusion that can be made from the comparison of RL and RIA dynamics is that the RIA levels observed in the 1-cm experiment cannot explain by itself the RL variation. We can deduce that in such short sample, the RIA is not dominating the RL response. In the case of 5-cm-long sample, the RL is correlated with the RIA evolution, which means that for such length, the RIA plays a major role on the RL signal output of the fiber. This is explained by the fact that the average distance traveled by the light in long samples is longer than that in short samples. Therefore, the impact of the RIA on the signal is more important.

When focusing on the spectral data, as shown in Fig. 3(a), the amplitude change of the RL highlighted in Fig. 2(a) is clearly noticeable. However, when the spectra are normalized to their maximum amplitude, it is observable that the change in amplitude is not supported by any noticeable change in the shape of the emission band even at doses of 600 kGy.

However, a slight change of shape is observable in long samples data, as shown in Fig. 3(b), which supports the idea of higher RIA effects in long samples.

B. Cu-Doped Fiber RL and RIA Measurements

In the case of Cu-doped fiber, the RL and RIA data are measured at 550 nm and shown in Fig. 4.

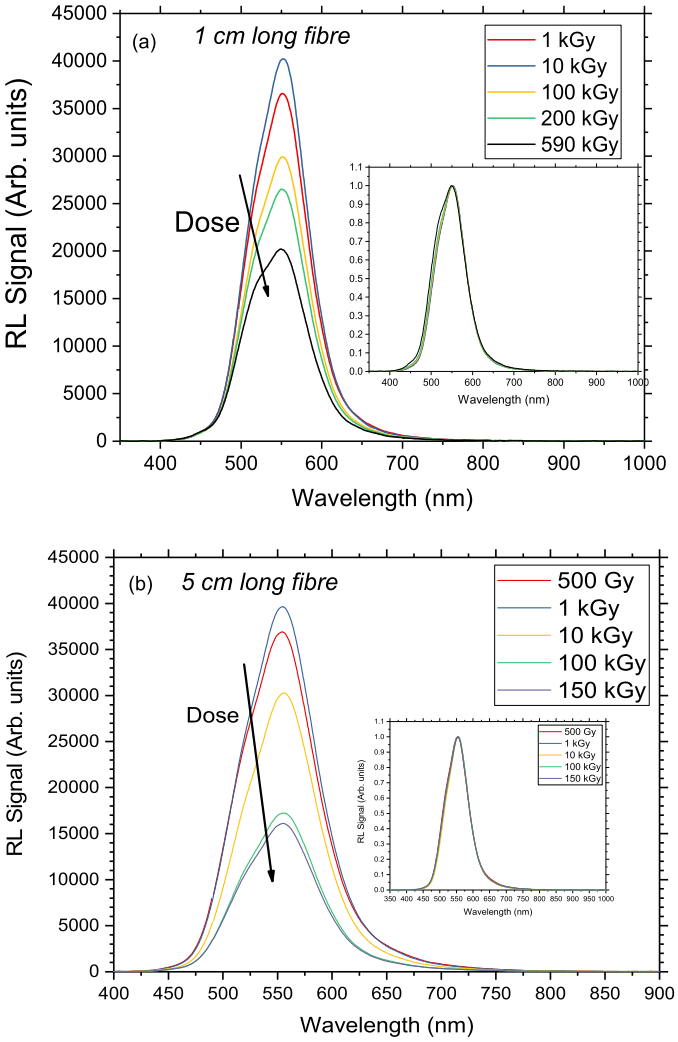

Fig. 5. RL spectrum measured on Cu-doped fiber for different TID levels shown as (a) 1-cm-long sample at 20 Gy/s and (b) 5-cm-long Ce-doped fiber at 5 Gy/s. Data are normalized to their own maximum amplitude in the insets.

In 1-cm-long sample testing reported in Fig. 4(a), we observe an increase of the RL signal until 3 kGy, then a decrease until the end of the irradiation. During the same irradiation, the RIA increases monotonically until becoming more stable toward the end of the irradiation within 2.3% variation on the RIA from 150 to 600 kGy.

For 5-cm-long samples, the dynamics of the RL is very similar. On the RIA side, we also observe a beginning of saturation at 100 kGy. One can also note the higher RIA levels observed in the Cu-doped fiber with respect to the Ce-doped fiber, with maximum RIA levels in the order of 180 and 250 dB/m, respectively.

In the same way as shown for Ce-doped fiber, we note that RIA impact on RL response is dominant only for the longer sample. When inspecting the spectral data, presented in Fig. 5(a), the amplitude change of the RL highlighted in Fig. 4(a) is clear. However, when the spectra are normalized to their maximum amplitude, it is observable that the change in amplitude is accompanied by a small change in the shape of the emission band. The shape of the spectrum below 520 nm seems to change slightly. The same effects are observed in long

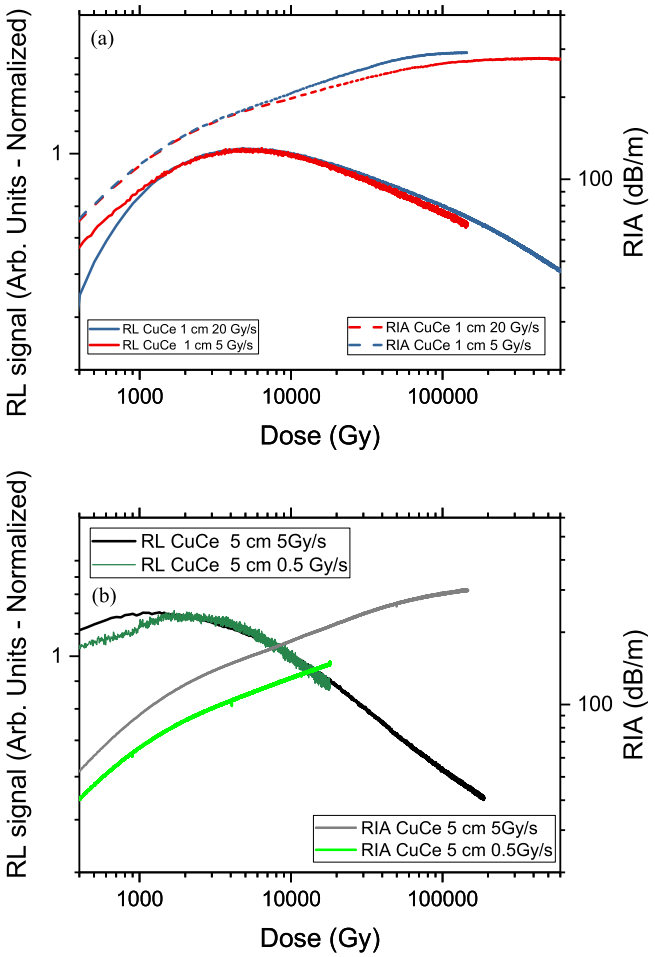

Fig. 6. RL and RIA measurement at 525 nm plotted versus dose on CuCe-codoped OF for (a) 1-cm-long and (b) 5-cm-long sample. RL data are normalized to the response at 10 kGy. Both RIA and RL presented in logarithmic scale.

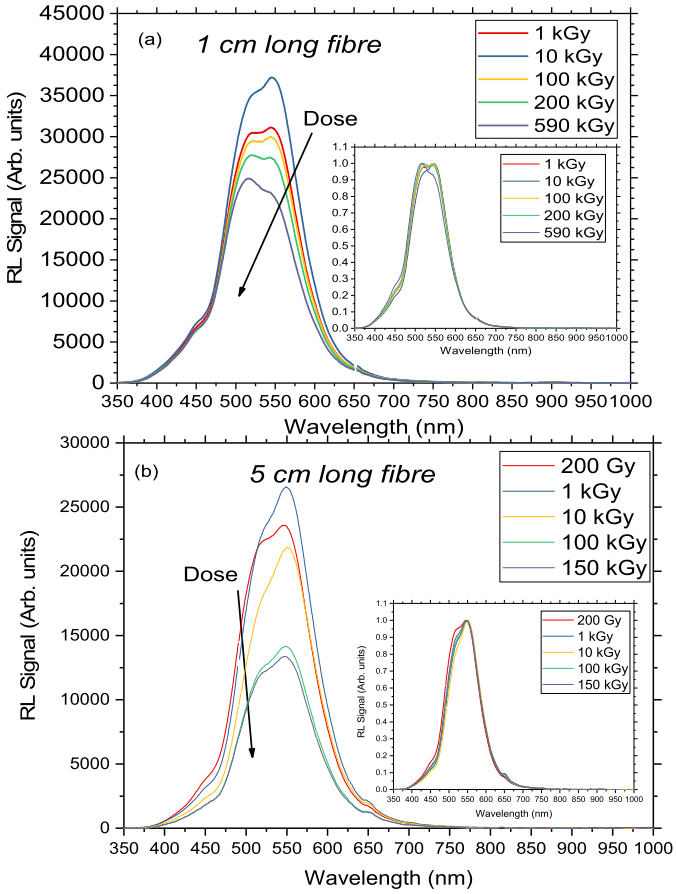

Fig. 7. RL spectrum measured on CuCe-codoped fiber for different TID levels shown as (a) 1-cm-long sample at 20 Gy/s and (b) 5-cm-long Ce-doped fiber at 5 Gy/s. Data are normalized to their own maximum amplitude in the insets.

sample data of Fig. 5(b), in a less important way because of the smaller final TID.

C. CuCe-Codoped Fiber RL and RIA Measurements

Later, the same characterization was performed on the CuCe co-doped fiber. The obtained data shown in Fig. 6 are measured around 525 nm.

In this fiber, the radiation response is analogous to that of the Cu-doped fiber. First, the RIA levels follow a similar trend and reach comparable amplitudes for both short and long sample lengths, with respect to that of Cu-doped fiber. Second, the RL signal also follows a similar trend as Cu-doped fiber. It is certainly explained by the presence of Cu dopants, which have a predominant effect on the overall response of the fiber due to its strong RIA contribution.

Regarding the spectral data, presented in Fig. 7(a), here again, the change of amplitude of the RL highlighted in Fig. 4(a) is clearly visible. Moreover, when the spectra are normalized to their maximum amplitude, an observation can be made: the change in amplitude is concomitant to a significant change in the shape of the emission band. This change is easily explained by the difference in the dynamics of the RL responses of Ce- and Cu-centers, as shown earlier in singly doped samples. Indeed, at the beginning of the irradiation (1 kGy), the maximum amplitude of the emission band is located at a wavelength compatible with copper ion centers (550 nm), whereas toward the end, the maximum amplitude is around the wavelength of the cerium ions (500 nm).

However, in long samples, we observe a faster decrease at lower wavelength of the spectra, which is compatible with higher RIA effects in long samples.

D. Gd-Doped Fiber RL Measurements

Whereas the OFs doped with Ce, Cu, or a combination of both compounds emit light in the visible domain, the Gd-doped fiber emits light around 314 nm. The RL signal data shown in Fig. 8 are measured at this wavelength.

In the 1-cm-long samples, it can be observed that the RL signal increases until 2 kGy and decreases slowly afterward. In between 2 and 100 kGy, the signal changes by less than 10%. However, in the 5-cm-long samples, we observed a different behavior. In the first part of the irradiation, the signal decreases strongly until 5 kGy before reducing much slower until 150 kGy. This could be explained by strong RIA effects in the UV region, more effective in this case because of the longer length of the sample. Unfortunately, due to experimental limitations, it was not possible to perform an RIA measurement in the UV-region on this fiber to verify this hypothesis.

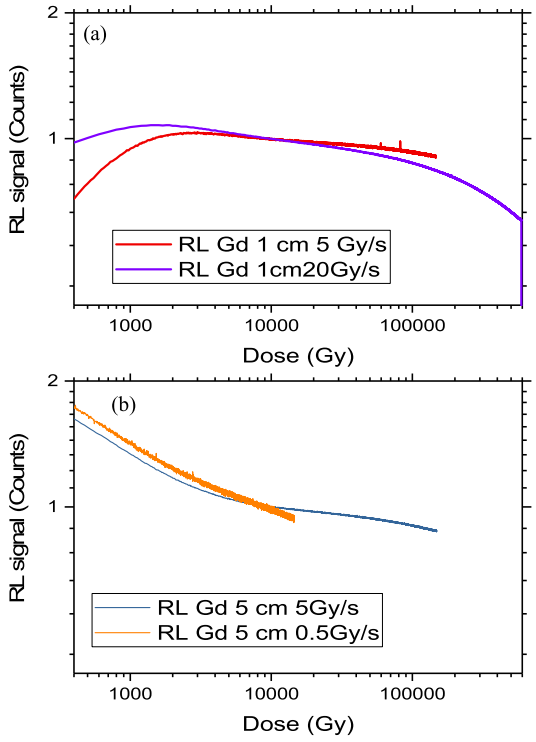

Fig. 8. RL and RIA measurements at 314 nm versus dose on Gd-doped OF for (a) 1-cm-long and (b) 5-cm-long sample. RL data are normalized to the response at 10 kGy.

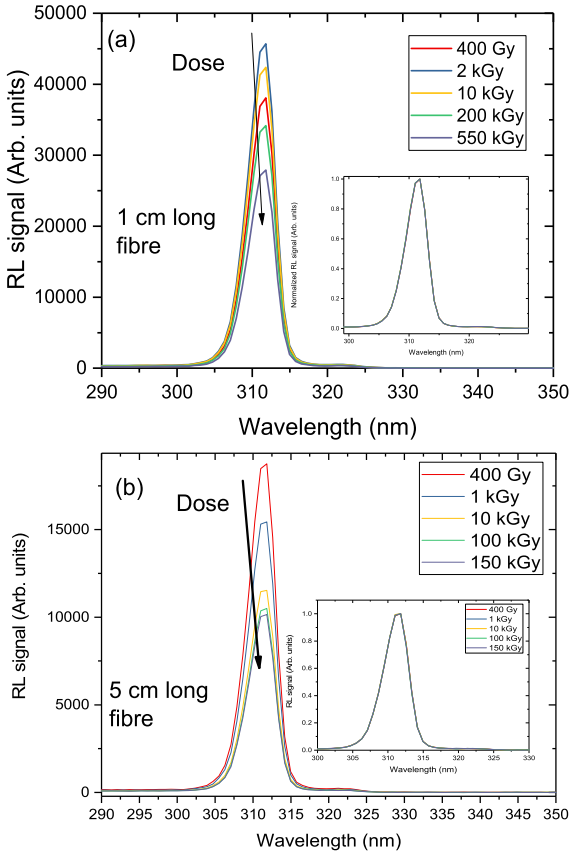

Fig. 9. RL spectrum measured on Gd-doped fiber for different TID levels shown as (a) 1-cm-long sample at 20 Gy/s and (b) 5-cm-long Ce-doped fiber at 5 Gy/s. Data are normalized to their own maximum amplitude in the inset.

When focusing on the spectral measurements displayed in Fig. 9(a), we can observe a sharp RL emission band peak centered at 314 nm and roughly 10 nm wide, characteristic of Gd centers. We also clearly notice the decrease of amplitude during the irradiation. At the same time, as shown in Fig. 9(b), when normalizing the spectra obtained at different TID, to their own maximum amplitude, we observe that there is no noticeable effect of the irradiation on the spectral shape of the emission.

E. RIA Spectral Data

To understand the impact of RIA effects on the RL, it is important to know the spectral distribution of this phenomenon. Generally, one can expect to have more RIA at smaller wavelength, which is the case for the investigated fibers.

In Fig. 10, we show the spectral data of the RIA measurements on the Ce- and Cu-doped and CuCe-codoped fibers, using a 1-cm-long sample, at a TID of 600 kGy (dose rate being 20 Gy/s). On the same figure, we also show the RL spectra of these fibers to highlight to what RIA these spectra are submitted.

One can notice in this figure that all spectra increase with decreasing wavelength illustrating the observation made in Figs. 3(a), 5(a), and 7(a), highlighting a noticeable impact of the left side of the spectra with increasing TID, on long samples. Additionally, the amplitude reached by Cu-doped and CuCe-codoped is significantly higher than that of Ce-doped fiber.

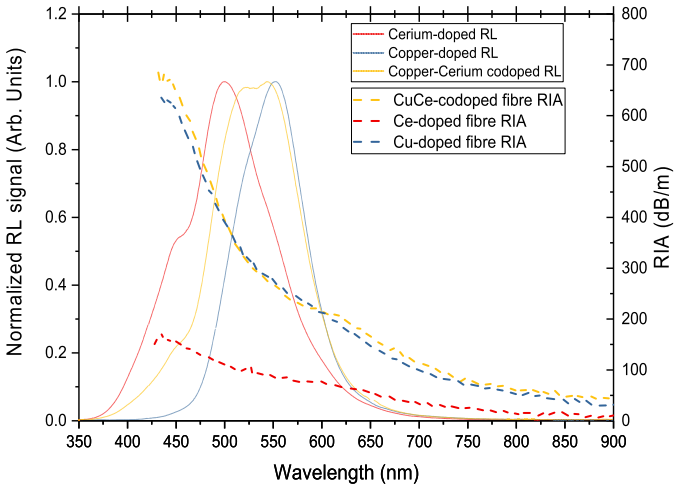

Fig. 10. RIA spectral responses and RL spectra measured on 1-cm-long Ce-doped, Cu-doped, and CuCe-codoped samples at a TID of 600 kGy under a dose rate of 20 Gy/s.

F. Ce- and Cu-Doped Fiber RL Responses After Recovery Time

In Fig. 11, it is interesting to note that when we start the second irradiation, the response of the Ce-doped and Cu-doped fibers restarts at the same level of the first irradiation (within 0.5% and 3%, respectively), after several hours recovery time.

However, even if the RL levels before and after irradiation are comparable, we can observe that the RL signal on the Cu-doped fiber increases by a few percentage, for a short time

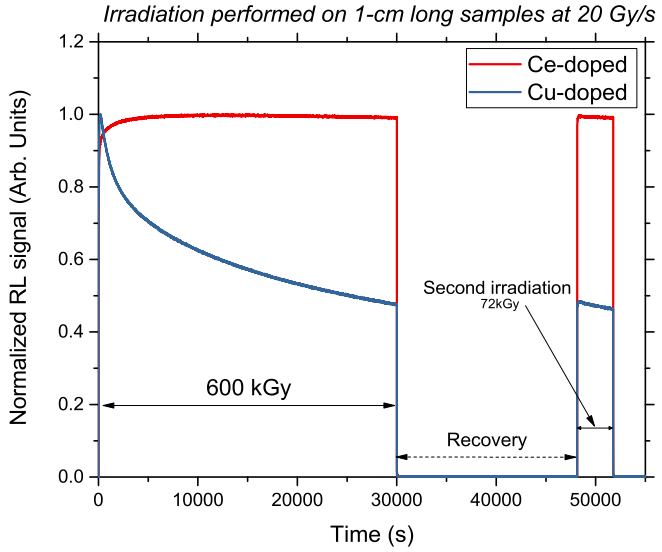

Fig. 11. RL measurements on 1-cm-long Ce- and Cu-doped samples at 20 Gy/s until 600 kGy, measured at 500 and 550 nm, respectively. After a recovery time of 5 h, a second irradiation of 72 kGy at the same dose rate is carried out. Both measurements are normalized to their own maximum amplitudes.

at the beginning of the second irradiation. This is probably due to some annealing effect occurring in the fiber during the recovery. Consequently, the Ce-doped fiber has the best performances in terms of stability of the RL signal during the first irradiation and compatibility of the amplitude before and after recovery.

IV. Discussion

In the fibers investigated in this work, we observe a simultaneous increase of the RL and RIA at the beginning of the irradiation run, which provides strong evidence of the increase of the RL efficiency of the fibers in this first phase. Indeed, at fixed dose rate if the RIA increases, an increase of the RL clearly can physically only be explained by an increase of the RL efficiency.

In the Ce-doped fiber, for 1-cm-long samples, the RL reaches a very stable response after 100 kGy, which is compatible with the fact that the RIA becomes also more stable. This stabilization of the RL response after a 100-kGy preirradiation is very interesting for dosimetry applications, because after this simple operation, the fiber keeps its stable response for several hundreds of kGy, after several hours of recovery time. This strongly suggests that this stabilization could work at long term. In other words, a preirradiation needs to be included in the calibration process of such sensors for future dosimetry applications, for doses higher than few tens of Gy. In addition, for long samples, we show that RIA plays a bigger role in the RL response dynamics than in short samples, because the emitted photons cross a longer path in the sample (on average) before collection by the transport fiber. Thus, making use of the highly efficient short OF sensor coupled with high efficiency detector is a better option to keep under control RIA effects.

In the Cu-doped fiber, we observe a decrease of the RL signal during the second phase of the irradiation (from 100 to 600 kGy). In some cases, this is explained by the fact that the RIA levels continue to increase, but in certain cases (see Fig. 4), we observe a decrease of the RL signal even when the RIA level becomes more stable. This observation strongly suggests a decrease of the RL efficiency in this fiber with increasing TID, at least after 100 kGy. Indeed, if the RIA remains stable while the RL decreases, it can only be explained by a decrease in RL efficiency.

The kinetics of the RL response in the CuCe-codoped fiber is similar to that observed in the Cu-doped fiber, which indicates that the Cu-dopants have a predominant effect in the overall response of the OF sensor. Additionally, spectral measurement in short samples has shown that the shape of the RL emission bands of both Ce- and Gd-doped fibers does not change significantly during the irradiation, whereas we observe a slight change in Cu-doped sample and a more important one in CuCe-codoped fiber. We can observe in this latter fiber a change of the RL emission spectrum due to the relative intensity changes of Cu- and Ce-centers emissions. This is highlighted by comparing the evolution of the RL spectra at several doses in CuCe-codoped and Ce- and Cu-doped fibers. Furthermore, spectral measurements on long samples support the idea of dominating RIA effects in long OF sensors.

The Gd-doped fiber has also shown strong dynamics in the RL response during the irradiation and a limited improvement in the stability of the response after a 100-kGy preirradiation (stable within 5% between 10 and 100 kGy). This stabilization is not comparable to the result obtained in Ce-doped fiber, where the preirradiation is more effective, over a larger dose range.

V. Conclusion and Outlook

We experimentally investigated the RL and RIA levels in differently doped OFs, for different fiber lengths, under different dose rates, to understand the combined effects of RIA and RL. A variation of the RL response with TID was observed in the tested fibers and is explained by combined RIA and RL efficiencies variations.

Furthermore, we identified a stabilization of the RL response of Ce-doped fiber after 100 kGy, which is very interesting from an application point of view, since it means that a preirradiation of the sample could allow the use of this fiber for radiation monitoring without significant change of its calibration. In addition, this effect remains effective after several hours of recovery, which indicates that this procedure could work over a long period of time.

The same effect was observed in the other fibers included in this study, but the 1-cm-long sample of Ce-doped fiber remains the best OF sensor candidate in terms of stability of the RL response during irradiation.

Acknowledgment

Hicham El Hamzaoui, Géraud Bouwmans, Andy Cassez, Bruno Capoen, and Mohamed Bouazaoui would like to thank FiberTech Lille platform for its technical support.

REFERENCES

[1] S. Girard et al., "Radiation effects on silica-based optical fibers: Recent advances and future challenges," *IEEE Trans. Nucl. Sci.*, vol. 60, no. 3, pp. 2015–2036, Jun. 2013.

[2] W. Primak, "Fast-neutron-induced changes in quartz and vitreous silica," *Phys. Rev.*, vol. 110, no. 6, pp. 1240–1254, Jun. 1958.

[3] B. Brichard, P. Borgermans, A. F. Fernandez, K. Lammens, and A. Decreton, "Radiation effect in silica optical fiber exposed to intense mixed neutron-gamma radiation field," *IEEE Trans. Nucl. Sci.*, vol. 48, no. 6, pp. 2069–2073, Dec. 2001.

[4] G. Pacchioni, L. Skuja, and D. L. Griscom, Eds., *Defects in SiO_2 and Related Dielectrics: Science and Technology*. Dordrecht, The Netherlands: Springer, 2000.

[5] S. Girard et al., "Integration of optical fibers in Megajoule class laser environments: Advantages and limitations," *IEEE Trans. Nucl. Sci.*, vol. 59, no. 4, pp. 1317–1322, Aug. 2012.

[6] D. L. Griscom, "Radiation hardening of pure-silica-core optical fibers: Reduction of induced absorption bands associated with self-trapped holes," *Appl. Phys. Lett.*, vol. 71, no. 2, pp. 175–177, Jul. 1997.

[7] D. Di Francesca et al., "O_2-loading treatment of Ge-doped silica fibers: A radiation hardening process," *J. Lightw. Technol.*, vol. 34, no. 9, pp. 2311–2316, May 1, 2016.

[8] D. Di Francesca et al., "Qualification and calibration of single-mode phosphosilicate optical fiber for dosimetry at CERN," *J. Lightw. Technol.*, vol. 37, no. 8, pp. 4643–4649, Sep. 15, 2019.

[9] A. Vedda et al., "Ce^{3+}-doped fibers for remote radiation dosimetry," *Appl. Phys. Lett.*, vol. 85, no. 26, pp. 6356–6358, Dec. 2004.

[10] N. Chiodini et al., "High-efficiency SiO_2: Ce^{3+} glass scintillators," *Appl. Phys. Lett.*, vol. 81, no. 23, pp. 4374–4376, Dec. 2002.

[11] I. Veronese et al., "Feasibility study for the use of cerium-doped silica fibres in proton therapy," *Radiat. Meas.*, vol. 45, nos. 3–6, pp. 635–639, Mar. 2010.

[12] S. Girard et al., "Potential of copper- and cerium-doped optical fiber materials for proton beam monitoring," *IEEE Trans. Nucl. Sci.*, vol. 64, no. 1, pp. 567–573, Jan. 2017.

[13] N. Al Helou et al., "Radioluminescence and optically stimulated luminescence responses of a cerium-doped sol-gel silica glass under X-ray beam irradiation," *IEEE Trans. Nucl. Sci.*, vol. 65, no. 8, pp. 1591–1597, Aug. 2018.

[14] H. El Hamzaoui et al., "Cerium-activated sol–gel silica glasses for radiation dosimetry in harsh environment," *Mater. Res. Exp.*, vol. 3, no. 4, Apr. 2016, Art. no. 046201.

[15] H. El Hamzaoui et al., "Gd^{3+}-doped sol-gel silica glass for remote ionizing radiation dosimetry," *OSA Contin.*, vol. 2, no. 3, pp. 715–721, Mar. 2019.

[16] J. Bahout et al., "Cu/Ce-Co-doped silica glass as radioluminescent material for ionizing radiation dosimetry," *Materials*, vol. 13, no. 11, p. 2611, Jun. 2020.

[17] R. G. Alía et al., "LHC and HL-LHC: Present and future radiation environment in the high-luminosity collision points and RHA implications," *IEEE Trans. Nucl. Sci.*, vol. 65, no. 1, pp. 448–456, Jan. 2018.

[18] S. Bourdarie and M. Xapsos, "The near-Earth space radiation environment," *IEEE Trans. Nucl. Sci.*, vol. 55, no. 4, pp. 1810–1832, Aug. 2008.

[19] D. Binder, E. C. Smith, and A. B. Holman, "Satellite anomalies from galactic cosmic rays," *IEEE Trans. Nucl. Sci.*, vol. NS-22, no. 6, pp. 2675–2680, Dec. 1975.

[20] D. M. Fleetwood, P. S. Winokur, and P. E. Dodd, "An overview of radiation effects on electronics in the space telecommunications environment," *Microelectron. Rel.*, vol. 40, no. 1, pp. 17–26, Jan. 2000.

[21] F. Moretti, G. Patton, A. Belsky, A. G. Petrosyan, and C. Dujardin, "Deep traps can reduce memory effects of shallower ones in scintillators," *Phys. Chem. Chem. Phys.*, vol. 18, no. 2, pp. 1178–1184, 2016.

[22] J. Vidalot et al., "Optical fiber-based monitoring of X-ray pulse series from a linear accelerator," *Radiation*, vol. 2, no. 1, pp. 17–32, Dec. 2021.

[23] N. Kerboub et al., "Temperature effect on the radioluminescence of Cu-, Ce-, and CuCe-doped silica-based fiber materials," *IEEE Trans. Nucl. Sci.*, vol. 68, no. 8, pp. 1782–1787, Aug. 2021.

[24] H. E. Hamzaoui et al., "Effects of densification atmosphere on optical properties of ionic copper-activated sol–gel silica glass: Towards an efficient radiation dosimeter," *Mater. Res. Exp.*, vol. 1, no. 2, Jun. 2014, Art. no. 026203.